Theor Chem Acc (2003) 110:10–18
DOI 10.1007/s00214-003-0440-8

Theoretical
Chemistry Accounts

Regular article

A kinetic stability study of MN_5 (M = Li, Na, K, and Rb)

Jun Fang Zhao, Nan Li, Qian Shu Li

The School of Chemical Engineering and Materials Science, Beijing Institute of Technology, Beijing 100081, China

Received: 20 October 2002 / Accepted: 13 January 2003 / Published online: 23 June 2003

Abstract. A structure and kinetic stability study on some complexes with the general formula MN_5, where M are the alkali-metal atoms, Li, Na, K, and Rb, has been carried by using hybrid density functional methods. Complex B (C_{2v}) with two points of attachment to the N_5 ring is the most energetically favored for all metals considered here. Pyramidal structures A (C_{5v}) are kinetically unstable and they rapidly rearrange to the most stable planar structures B. At the QCISD(T)/6-311 + G*//B3LYP/6-311 + G* + ZPE (B3LYP/6-311 + G*) level, the decomposition barrier heights of LiN_5-B, NaN_5–B, KN_5-B, and RbN_5-B are predicted to be 19.9, 22.0, 22.5, and 23.0 kcal/mol, respectively. In addition, the rate constants of the decomposition reaction MN_5-B $\rightarrow MN_3 + N_2$ (M = Li, Na, K, and Rb) are also predicted using conventional transition state theory and canonical variational transition state theory, respectively.

Keywords: Kinetic stability – Density functional theory calculations – MN_5 complex

Introduction

In recent years, polynitrogen and nitrogen-rich compounds have been the subjects of intense and sustained experimental and theoretical scrutiny [1, 2, 3, 4, 5, 6, 7, 8, 9, 10]. In addition to the fundamental significance of these molecules, such extraordinary interests are motivated by the potential use as high-energy density materials that are environmentally acceptable. However, owing to the highly endothermic heats of formation, their syntheses and handling have been great challenges for experimental chemists. The successful synthesis of stable salts of the N_5^+ cation [11], the third experimental known all-nitrogen compound from the three last centuries, has inspired greatly many research groups to search for other stable polynitrogen species. Recently, Cacace et al. [12] demonstrated the existence of the tetranitrogen molecule, N_4, as a metastable species with a lifetime exceeding 1 μs at 298 K. Most recently, Vij et al. [13] reported the first experiment detection of the long-sought pentazolate anion by cleaving the C–N bond of suitably substituted phenylpentazoles. The new discoveries indicate a bright future for experimental polynitrogen chemistry.

The successful detection of N_5^- holds great promise for the bulk synthesis of N_5^- salts. Some theoretical studies of substituted pentazoles have been carried out. Previously, Ferris and Bartlett [14] investigated theoretically the stability and vibrational properties of the pentazoles HN_5 using coupled-cluster and many-body perturbation theory (MBPT). Glukhovtsev et al. [15] reported the structures and stability for its lithium derivatives (N_5Li) by using ab initio methods. Nguyen et al. [16] carried out extended Hückel theory calculations of $TM(CO)_3(\eta^5\text{-}N_5)$ with $TM = Fe^{2+}$, Mn, and Cr^-, which suggested that the pentazole complexes would be formed if the fragments could be brought together. Recently, Gagliardi and Pyykkö [17, 18] have predicated the possible existence of two new classes of compounds, $Sc(\eta^7\text{-}N_7)$ and $\eta^5\text{-}N_5^-\text{–}M\text{–}\eta^7\text{-}N_7^{3-}$, where the N_5^- and N_7^{3-} are stabilized as planar rings by the interaction of their π system with a transition metal atom (M) in the η^5 and η^7 bonds. Lein et al. [19] predicted that the ferrocene-like $Fe(\eta^5\text{-}N_5)$ is a strongly bonded complex which has D_{5d} symmetry. Burke et al. [20] performed theoretical characterization of pentazole anion with metal counterions, where the metals considered are Na, K, Mg, Ca, and Zn by using ab initio and density functional methods. With these alkali (Na, K), alkaline-earth (Mg, Ca) and group IIB (Zn) metals, it is expected that the metal–pentazole complexes would be predominantly ionic in nature and that elec-

Correspondence to: Q. S. Li
e-mail: qsli@mh.bit.edu.cn

trostatic interaction would dominate. Moreover, they also pointed out that the nature of the cation has an influence on the electronic, vibrational, and NMR spectra of the pentazole anion. The stability of these compounds towards dissociation was, however, not studied. To assess their kinetic stability further, in this paper, we provide a theoretical investigation on the decomposition and isomerization pathways for some complexes with general formula MN_5, where M are the alkali-metal atoms Li, Na, K, and Rb, with the intention to support experimental studies on the pentazole derivatives.

Calculation methods

The calculations were carried out with the Gaussian 98 program system [21]. All structures, energies, and vibrational data were calculated by density functional theory (DFT) methods. The DFT functions used in the present work include B3LYP (B3 and the nonlocal correlation of Lee, Yang, and Parr) [22, 23] and B3PW91 (Beck's three-parameter hybrid functional and Perdew and Wang's 1991 gradient-corrected correlation functional) [24]. The 6-311 + G* basis sets were used for the nitrogen atoms and metal atoms, M = Li, Na, and K. When M belongs to the fourth row of the periodic table, M = Rb, effective core potentials (ECPs) were used on the metal atom, and the energy-adjusted Stuttgart ECPs [25, 26, 27] were used for this purpose. Vibrational frequencies at the above levels were used to characterize stationary points as minima (number of imaginary frequencies (NIMAG = 0) or transition states (NIMAG = 1) and to evaluate zero-point vibrational energies (ZPEs). Minimum-energy pathways connecting the reactants and products were confirmed using the intrinsic reaction coordinate (IRC) method with the Gonzalez–Schlegel second-order algorithm [28, 29]. Final energies were further calculated at the QCISD(T)/6-311 + G*//B3LYP/6-311 + G* level of theory. In addition, in order to gain more information on the electronic properties, the natural bond orbital (NBO) analysis [30, 31] was performed at the B3LYP/6-311 + G* level of theory using the optimized geometry at the same level.

The POLYRATE 8.2 [32] program was employed to evaluate the reaction rate constant at various temperatures. For propose of comparison, calculations of the reaction were carried out by the conventional transition-state theory (TST) and canonical variational TST (CVT). The latter is based on varying the dividing surface along a reference path to minimize the rate constant. The CVT rate constants were also corrected using the small-curvature tunneling (SCT) transmission coefficient [33, 34]; this is based on the centrifugal-dominant small-curvature semiclassical adiabatic ground state method.

Throughout this paper, bond lengths are given in angströms, bond angles in degrees, total energies in hartrees, relative and zero-point vibrational energies, unless otherwise stated, in kilocalories per mole.

Results and discussion

As previous studies [15, 20] have pointed out, from the structural point of view, Li, Na, K, and Rb can bond with the N_5 ring to form three kinds of structure: pyramidal A, planar B and C (Scheme 1).

The geometric structures of stationary points, transition states, and dissociated products for LiN_5, NaN_5, KN_5, and RbN_5 are plotted in Figs. 1, 2, 3, and 4, respectively. The total energies, ZPEs, and lowest vibrational frequencies are listed in Tables 1, 2, 3, and 4, respectively. Relative energies are summarized in Tables 5, 6, 7, and 8, respectively.

LiN_5

Similar to the well-documented pyramidal structure of lithium cyclopentadienide, $(CH)_5Li$, pyramidal LiN_5 with C_{5v} symmetry A is a stable point on the DFT potential-energy surface; however, it is 8.2 kcal/mol higher in energy than the planar structure LiN_5-B with C_{2v} symmetry (Table 5). The planar structure containing monocoordinated lithium LiN_5-TS-C is not a stable isomer with an imaginary frequency. IRC calculations performed at the B3LYP and B3PW91 levels verify that it corresponds to the transition state for the Li transfer around the N_5 ring. Energetically LiN_5-TS-C lies 4.8 kcal/mol above the stable LiN_5-B at the QCISD(T) level, in contrast to 6.7 kcal/mol at the MP4SDTQ/6-31 + G*//MP2/6-31G* level [15]. As shown in Fig. 1, the N–N bond lengths are equivalent in LiN_5-A and they are close to the N–N distances in the isolated N_5^-anion (1.326 Å at the B3LYP/6311 + G* level), indicating that the N_5^- anion preserves its structural integrity in forming the LiN_5-A complex. However, in LiN_5-B and LiN_5-TS-C, the presence of the metal cation on the side of the ring induces alternating bond lengths, and thus less aromatic character. Our kinetic analyses show that the pyramidal structure LiN_5-A is not kinetically stable enough. A transition state TS1 corresponding to rearrangement to the most stable planar isomer LiN_5-B was found and characterized with only one imaginary frequency at the DFT levels. IRC calculations confirm that TS1 does connect two minima LiN_5-A and LiN_5-B on the potential-energy surface. At the QCISD(T) level, TS1 is only 2.0 kcal/mol higher in energy than LiN_5-A, indicating that the pyramidal structure LiN_5 (C_{5v}) possesses significant kinetic instability. On the other hand, the unimolecular decomposition pathway of the most stable isomer LiN_5-B has also been examined at the DFT levels. The decomposition process of LiN_5-B $\rightarrow$ TS2(C_S) $\rightarrow$ $LiN_3(C_{\infty v}) + N_2$ proceeds through the LiN_5 complex ($C_{\infty v}$) as indicated by the IRC calculation performed at the B3LYP and B3PW91 levels of theory. Our results show linear that the LiN_5 complex, shown in Fig. 1, is a minimum on the potential-energy surface with all-real vibrational frequencies. The LiN_5 complex is 35.6 kcal/mol more stable than B at the QCISD(T) level. On the basis of the energy difference between LiN_5-B and TS2, the decomposition barrier height is predicted to be 19.9 kcal/mol at the QCISD(T) level (Table 5), in contrast to 16.2 kcal/mol computed by Ferris and Bartlett [14] at the MBPT(2)/DZP level of theory. A previous study [35] suggested that the diffuse functions substantially reduce basis set superposition error (BSSE) effects, and our calculations also show the BSSE correction is relatively small (less than 5% of the binding energy). Therefore, in the present work, the binding energies were computed by neglecting BSSE. As

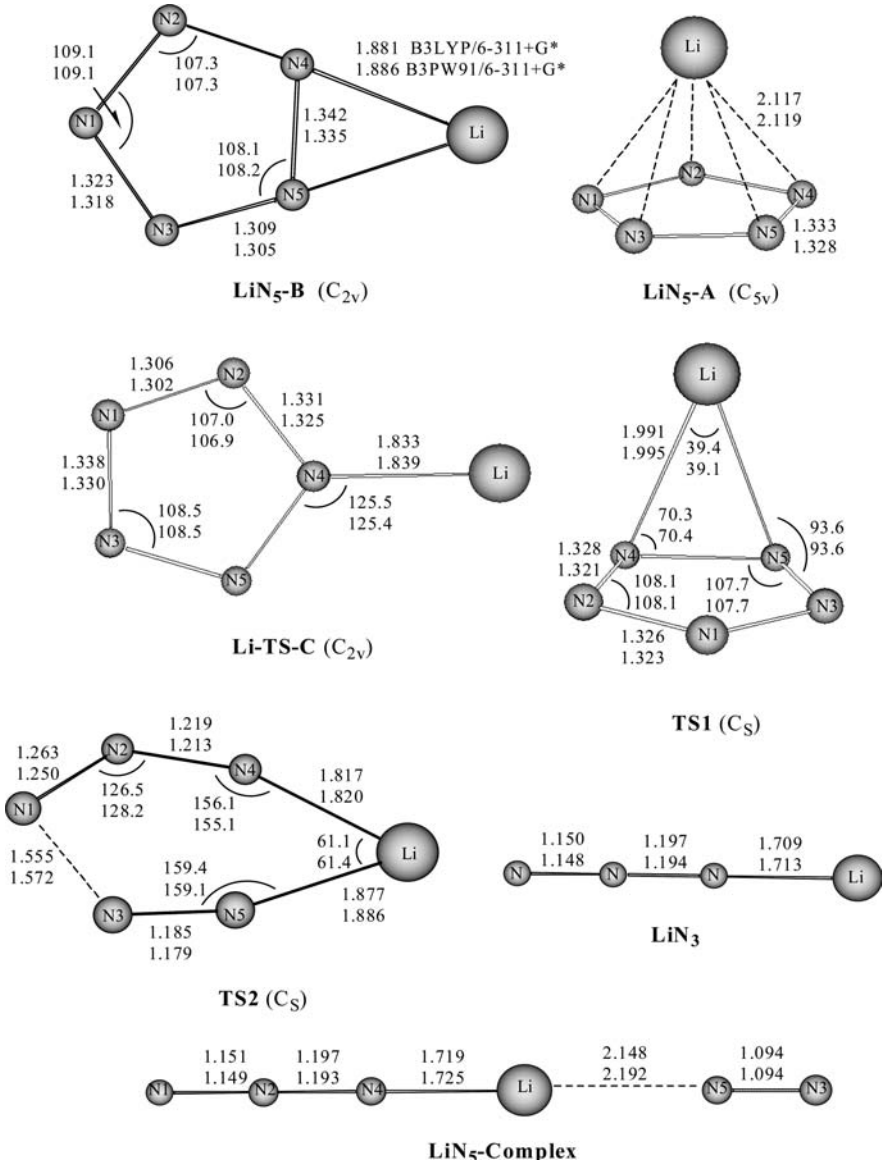

Fig. 1. Optimized molecular structures and transition states for LiN_5

can be seen in Table 5, the binding energy of the LiN_5 complex is predicted to be 6.2 kcal/mol at the QCISD(T) level. Glukhovtsev et al. [15] have pointed out that the linear structure is the most stable LiN_3 isomer. As shown in Fig. 1, the bond length of Li–N is 1.709 Å at the B3LYP/6-311 + G* level of theory. In terms of NBO analysis, the calculated Wiberg bond index of Li–N is close to zero. Furthermore the positive charges reside on the Li atom. Therefore, this compound would be predominantly ionic in nature and electrostatic interaction would dominate.

NaN_5 and KN_5

Similar to the LiN_5 situation, the planar structures NaN_5-B and KN_5-B with C_{2v} symmetry are the lowest-energy isomers on their respective potential-energy surface at the B3LYP and B3PW91 levels of theory. The pyramidal structures A with C_{5v} symmetry are 5.7 and 1.6 kcal/mol higher in energy than B at the QCISD(T) level, respectively, as shown in Tables 6 and 7. TS3 (C_S) and TS5 (C_S) corresponding to isomerization reaction from A to B have been located at the DFT level. Energetically TS3 and TS5 are only 0.7 and 2.7 kcal/mol higher than A at the QCISD(T) level of theory. The very low barrier heights indicate that pyramidal NaN_5-A and KN_5-A are not likely to be stable and they will rapidly rearrange to NaN_5-B and KN_5-B. Similar to LiN_5, NaN_5-TS-C and KN_5-TS-C are also transition states corresponding to the Na and K transfer around the N_5 ring. The energy differences between TS-C and B are 4.0 and 5.1 kcal/mol at the QCISD(T) level, respectively. The decomposition mechanism of the most stable isomers, NaN_5-B and KN_5-B, were also investigated in our present work by using DFT methods. We have located two transition structures, TS4 and TS6, with C_S symmetry, as shown in Figs. 2 and 3, at the B3LYP and

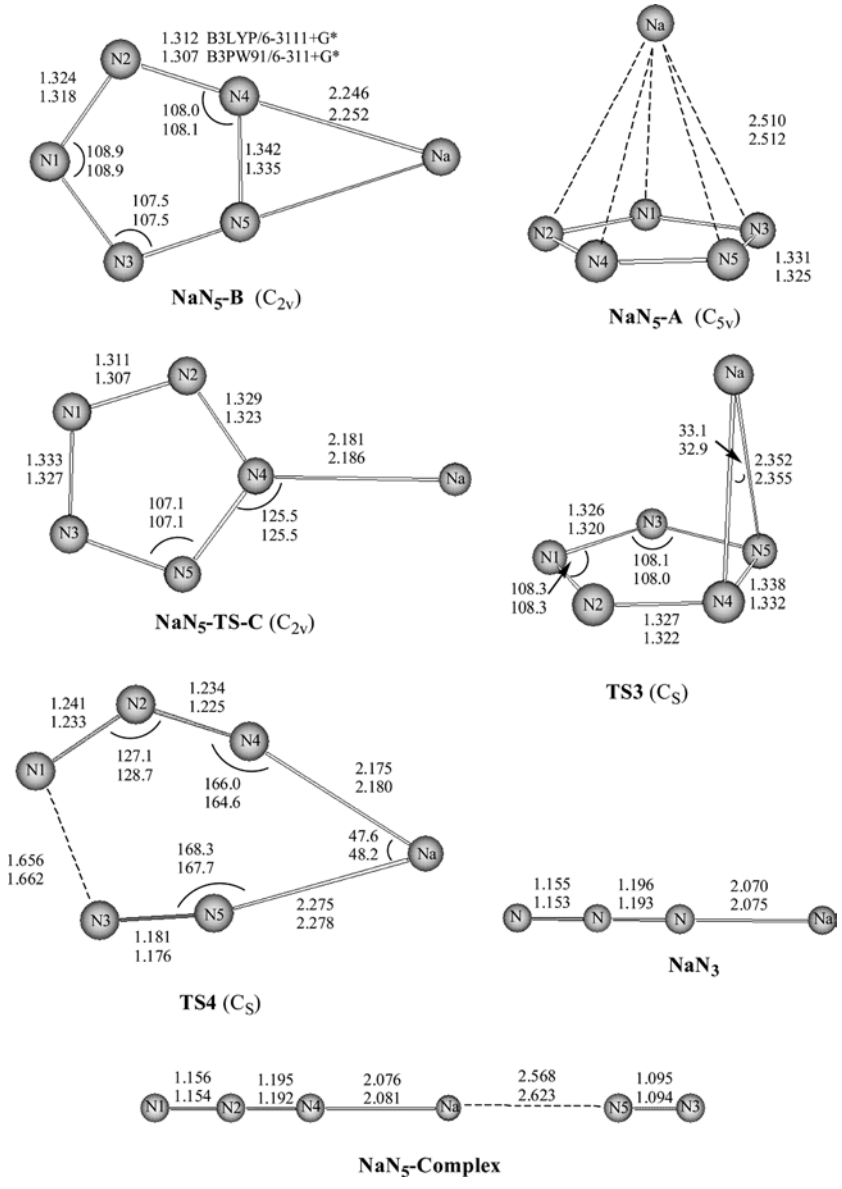

Fig. 2. Optimized molecular structures and transition states for NaN_5

B3PW91 levels of theory. The barrier heights for the decomposition reactions NaN_5-B → TS4 → NaN_5 complex → NaN_3 ($C_{\infty v}$) + N_2 and KN_5-B → TS6 → KN_5 complex → KN_3 ($C_{\infty v}$) + N_2 are predicated to be 22.0 and 22.5 kcal/mol at the QCISD(T) level, respectively, indicating a higher kinetic stability than LiN_5-B. From Tables 6 and 7, the binding energies of the NaN_5 complex and the KN_5 complex are 4.1 and 3.2 kcal/mol at the QCISD(T) level without BSSE correction.

RbN_5

Given the increasing stability in going from lighter to heavier metals (from Li to K), we investigated the possible structures and stability of Rb complex with pentazole. We are not aware of any studies on the role of relativistic effects on the bonding of the heavier metals to 6π aromatic rings. As shown in Fig. 4 and Table 8, the planar RbN_5-B with two points of attachment to the ring and the pyramidal RbN_5-A, are local minima on the potential-energy surface at the DFT levels of theory. RbN_5-B is more stable than RbN_5-A by only 1.3 kcal/mol at the QCISD(T) level. RbN_5-TS-C is also a transition state corresponding to the metal atom Rb transfer around the N_5 ring with a low barrier height, 4.2 kcal/mol at the QCISD(T) level, shown in Table 8. The possible isomerization from RbN_5-A to RbN_5-B and the dissociation pathways for RbN_5-B were investigated, in analogy with what was done for NaN_5 and KN_5. As seen in Table 8, the low barrier heights of the isomerization reaction suggest that the pyramidal isomer RbN_5-A is also kinetically unstable. However, the dissociation barrier height of RbN_5-B is predicted to be 23.0 kcal/mol at the QCISD(T) level, indicating a little higher kinetic stability than that of NaN_5 and KN_5. NBO analysis suggests that the more electropositive the metal atom is, the less influence on the electronic structure of

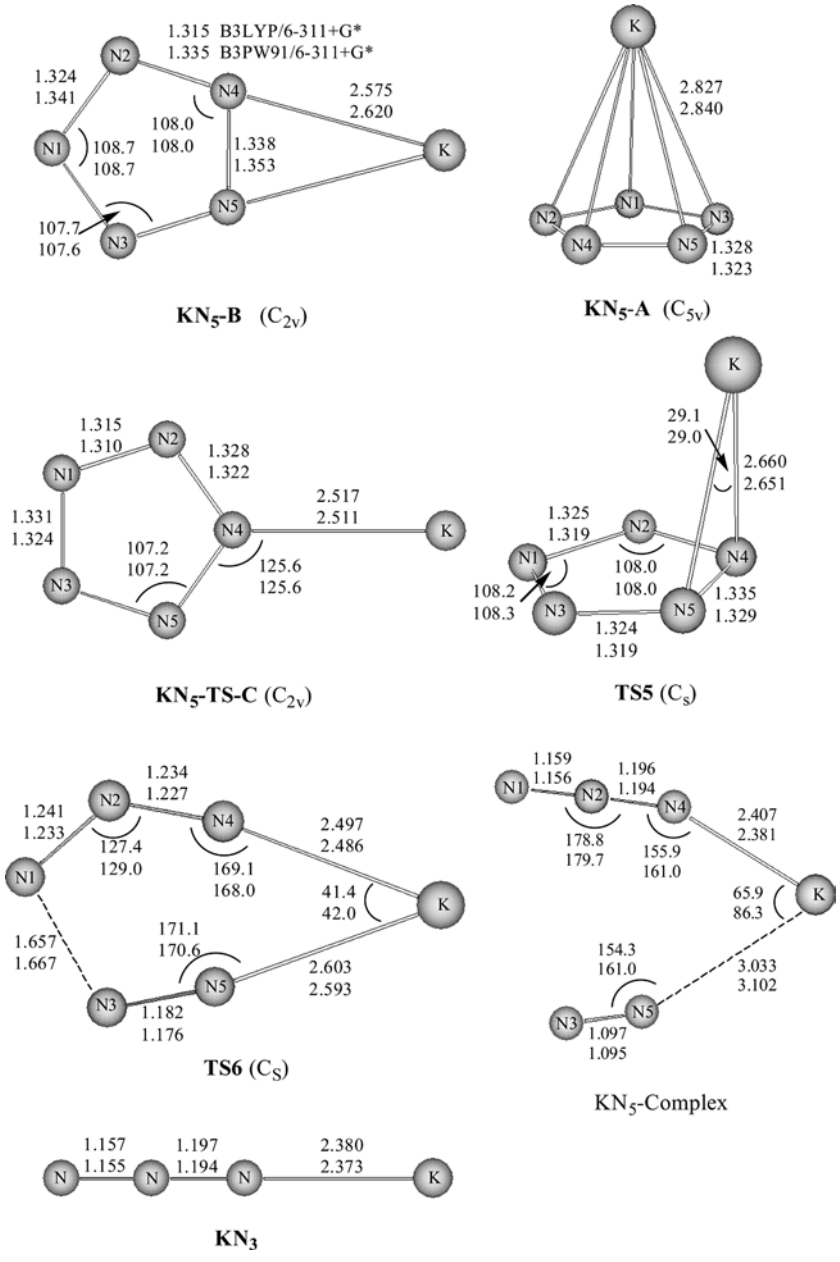

Fig. 3. Optimized molecular structures and transition states for KN_5

the anion N_5^- ring would have. The decomposition barrier of the isolated cyclic N_5^- (D_{5h}) is 25.8 kcal/mol at the QCISD(T)/6-311 + G*//B3LYP/6-311 + G* + ZPE (B3LYP/6-311 + G*) level. Therefore, RbN_5-B presents the highest decomposition barrier height with the highest electropositivity among the metals considered here. The binding energy of RbN_5 complex is 3.1 kcal/mol at the QCISD(T) level without BSSE correction (Table 8).

The rate constants for the decomposition reactions MN_5-B → $MN_3 + N_2$

The rate constants for the decomposition reactions MN_5-B → $MN_3 + N_2$ (M = Li, Na, K, and Rb) were calculated by using POLYRATE 8.2. For the purpose of comparing the rate constants of the decomposition reactions, the rate constants using the TST, CVT, and CVT/SCT methods were calculated, as shown in Tables 9, 10, 11, and 12. It is observed that the TST and CVT rate constants are quite close to each other, indicting that the variational effects are very small. It can be seen that the rate constants of CVT/SCT are larger than those of TST and CVT. These results imply that the SCT corrections are required. From the discussion, we conclude that the theoretical CVT/SCT rate constants appear probably more reliable.

Summary

A theoretical study on the structures and decomposition pathways of some complexes with general formula MN_5,

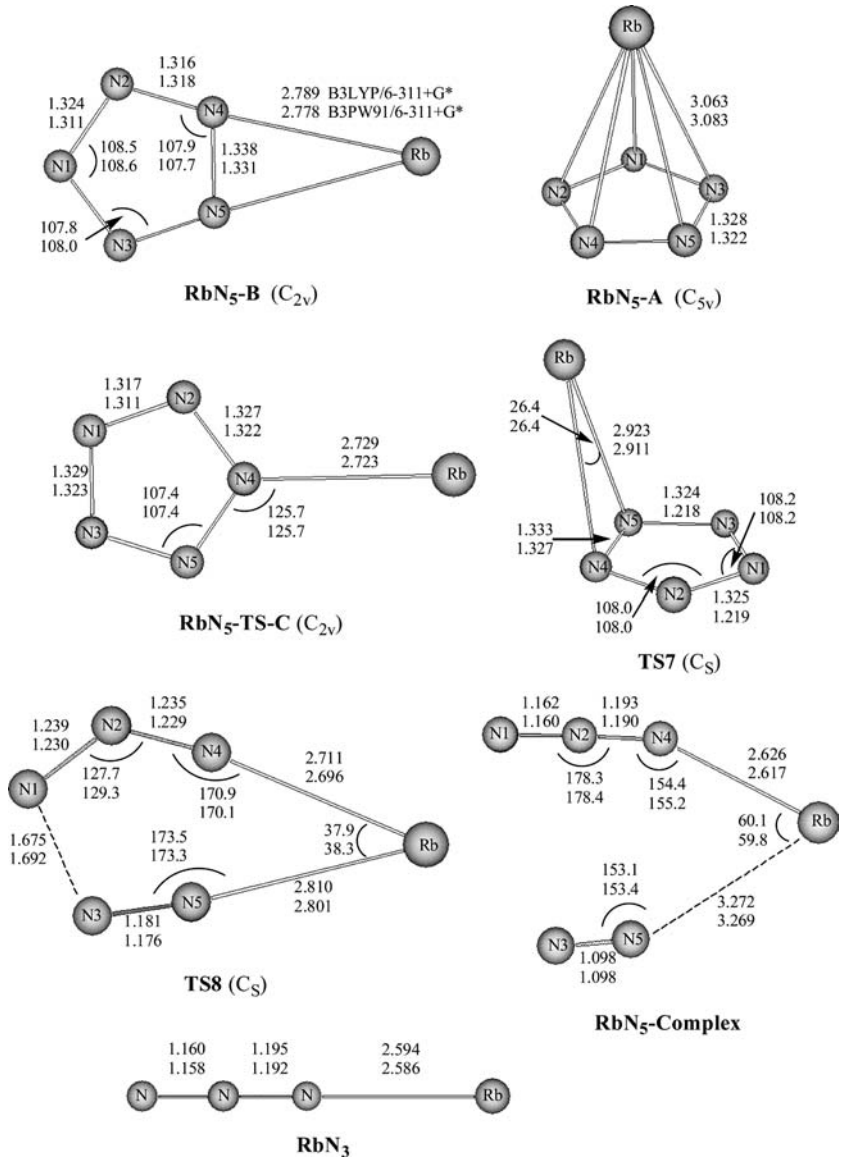

Fig. 4. Optimized molecular structures and transition states for RbN_5

Table 1. The total energies, E, (hartrees) zero-point energies (ZPE) (kcal/mol), and the lowest vibrational frequencies, ν_1, (1/cm) for LiN_5

Species	B3LYP/6-311 + G*			B3PW91/6-311 + G*			QCISD(T)/6-311 + G*[a]
	E	ZPE	ν_1	E	ZPE	ν_1	
LiN_5-A	−281.3101901	14.6	220	−281.1930631	14.8	220	−280.6154408
TS1	−281.3068795	14.3	−179	−281.1897688	14.6	−180	−280.6118276
LiN_5-B	−281.3272833	15.0	158	−281.2096106	15.3	160	−280.6291645
LiN_5-TS-C	−281.3186353	14.7	−72	−281.2012945	15.0	−72	−280.6209629
TS2	−281.2969897	13.2	−588	−281.1731813	13.3	−601	−280.5945281
LiN_5 complex	−281.3829766	12.8	22	−281.2521701	12.8	25	−280.6824673
LiN_3 ($C_{\infty v}$)	−171.8130923	8.8	159	−171.7333731	8.9	140	−171.3564558
$LiN_3 + N_2$	−281.372786	12.3	–	−281.2433854	12.4	–	−280.6716872

[a]Single-point energy at the QCISD(T)/6-311 + G*//B3LYP/6-311 + G* level

where M are the alkali metal atoms, Li, Na, K, and Rb, has been carried by using hybrid DFT methods. Similar to the pyramidal structure of lithium cyclopentadienide— $(CH)_5Li$, pyramidal LiN_5-A, NaN_5-A, KN_5-A, and RbN_5-A are all local minima on their respective potential-energy surfaces. However, the low barrier heights suggest that the pyramidal structures are kinetically unstable and they will rapidly rearrange to the

Table 2. E (hartrees), ZPE (kcal/mol), and ν_1 (1/cm)] for NaN_5

Species	B3LYP/6-311 + G*			B3PW91/6-311 + G*			QCISD(T)/6-311 + G*[a]
	E	ZPE	ν_1	E	ZPE	ν_1	
NaN_5-A	−436.0854426	14.0	100	−435.9334256	14.3	100	−435.0143676
TS3	−436.0842851	13.9	−92	−435.9322044	14.2	−92	−435.0131089
NaN_5-B	−436.0976466	14.4	101	−435.9449784	14.7	101	−435.0241448
NaN_5-TS-C	−436.0903363	14.1	−80	−435.9378079	14.4	−80	−435.0172329
TS4	−436.0627712	12.4	−626	−435.9038658	12.6	−629	−434.9859489
NaN_5 complex	−436.1412781	11.8	12	−435.9763382	11.9	13	−435.0660565
NaN_3 ($C_{\infty v}$)	−326.5750104	7.9	82	−326.4607663	8.0	93	−325.7436615
$NaN_3 + N_2$	−436.1347041	11.4	–	−435.9707786	11.5	–	−435.0588929

[a]Single-point energy at the QCISD(T)/6-311 + G*//B3LYP/6-311 + G* level

Table 3. E (hartrees), ZPE (kcal/mol), and ν_1 (1/cm) for KN_5

Species	B3LYP/6-311 + G*			B3PW91/6-311 + G*			QCISD(T)/6-311 + G*[a]
	E	ZPE	ν_1	E	ZPE	ν_1	
KN_5-A	−873.7429727	14.0	108	−873.5777658	14.3	113	−872.5197863
TS5	−873.7401888	13.9	−81	−873.5748494	14.2	−82	−872.5153886
KN_5-B	−873.7488963	14.2	81	−873.5834033	14.5	80	−872.522683
KN_5-TS-C	−873.7409749	14.0	−79	−873.5755666	14.2	−79	−872.5141748
TS6	−873.7130277	12.2	−626	−873.5412832	12.4	−630	−872.4836676
KN_5 complex	−873.7872345	11.6	13	−873.6103344	11.7	15	−872.5598474
KN_3 ($C_{\infty v}$)	−764.2244047	7.6	79	−764.0974585	7.7	74	−763.2387439
$KN_3 + N_2$	−873.7840984	11.1	–	−873.6074708	11.2	–	−872.5539753

[a]Single-point energy at the QCISD(T)/6–311 + G*//B3LYP/6-311 + G* level

Table 4. E (hartrees), ZPE (kcal/mol), and ν_1 (1/cm) for RbN_5

Species	B3LYP/6-311 + G*[a]			B3PW91/6-311 + G*[a]			QCISD(T)/6-311 + G*[a, b]
	E	ZPE	ν_1	E	ZPE	ν_1	
RbN_5-A	−297.9087066	13.9	87	−297.587828	14.1	89	−297.0078248
TS7	−297.906573	13.8	−63	−297.8187236	14.1	−64	−297.0047403
RbN_5-B	−297.913045	14.1	68	−297.8250096	14.4	66	−297.0100219
RbN_5-TS-C	−297.9060848	13.8	−72	−297.8180564	11.1	−71	−297.0028677
TS8	−297.8763295	12.0	−626	−297.7820203	12.2	−630	−296.9699849
RbN_5 complex	−297.9482854	11.6	58	−297.8482433	11.7	55	−297.0445923
RbN_3 ($C_{\infty v}$)	−188.3851816	7.4	54	−188.3357366	7.5	54	−187.7242998
$RbN_3 + N_2$	−297.9448753	10.9	–	−297.8457489	11.0	–	−297.0395312

[a]The 6-311 + G* basis set was used for N atoms and the effective core potentials were used for the Rb atom
[b]Single-point energy at the QCISD(T)/6-311 + G*//B3LYP/6-311 + G* level

Table 5. The relative energies (kcal/mol) for LiN_5

Species	B3LYP/ 6-311 + G*	B3PW91/ 6-311 + G*	QCISD(T)/ 6-311 + G*[a]
LiN_5-A	10.3	9.9	8.2
TS1	12.1	11.8	10.2
LiN_5-B	0.0	0.0	0.0
LiN_5-TS-C	5.1	4.9	4.8
TS2	17.2	20.9	19.9
LiN_5 complex	−37.1	−29.2	−35.6
$LiN_3 + N_2$	−31.3	−24.1	−29.4

[a]Relative energies at the QCISD(T)/6-311 + G*//B3LYP/6-311 + G* + ZPE(B3LYP/6-311 + G*) level

most stable planar structures B. At our QCISD(T)/6-311 + G*//B3LYP/6-311 + G* level, the decomposition barrier heights of LiN_5-B, NaN_5-B, KN_5-B, and RbN_5-B are predicted to be 19.9, 22.0, 22.5 and 23.0 kcal/mol, respectively. In addition, rate constants using TST, CVT, and CVT/SCT calculations for the decomposition reactions $MN_5\text{-B} \rightarrow MN_3 + N_2$ were performed. The calculated results imply that the SCT corrections are necessary in computing the rate constants of these decomposition reactions. Therefore, we predicted that the theoretical CVT/SCT rate constants are probably more reliable.

Table 6. The relative energies (kcal/mol) for NaN_5

Species	B3LYP/ 6-311+G*	B3PW91/ 6-311+G*	QCISD(T)/ 6-311+G*[a]
NaN_5-A	7.3	6.8	5.7
TS3	7.9	7.5	6.4
NaN_5-B	0.0	0.0	0.0
NaN_5-TS-C	4.3	4.2	4.0
TS4	19.9	23.7	22.0
NaN_5 complex	−30.0	−22.5	−28.9
NaN_3+N_2	−26.3	−19.4	−24.8

[a]Relative energies at the QCISD(T)/6-311+G*//B3LYP/6-311+G*+ZPE(B3LYP/6-311+G*) level

Table 7. The relative energies (kcal/mol) for KN_5

Species	B3LYP/ 6-311+G*	B3PW91/ 6-311+G*	QCISD(T)/ 6-311+G*[a]
KN_5-A	3.5	3.3	1.6
TS5	5.2	5.1	4.3
KN_5-B	0.0	0.0	0.0
KN_5-TS-C	4.8	4.6	5.1
TS6	20.5	24.3	22.5
KN_5 complex	−26.7	−19.7	−25.9
KN_3+N_2	−25.2	−18.4	−22.7

[a]Relative energies at the QCISD(T)/6-311+G*//B3LYP/6-311+G*+ZPE(B3LYP/6-311+G*) level

Table 8. The relative energies (kcal/mol) for RbN_5

Species	B3LYP/ 6-311+G*[a]	B3PW91/ 6-311+G*[a]	QCISD(T)/ 6-311+G*[a,b]
RbN_5-A	2.1	1.9	1.3
TS7	3.4	3.3	3.1
RbN_5-B	0.0	0.0	0.0
RbN_5-TS-C	4.0	4.0	4.2
TS8	21.0	24.8	23.0
RbN_5 complex	−24.6	−17.3	−24.2
RbN_3+N_2	−22.7	−15.9	−21.1

[a]The 6-311+G* basis set was used for N atoms and the effective core potentials were used for the Rb atom
[b]Relative energies at the QCISD(T)/6-311+G*//B3LYP/6-311+G*+ZPE(B3LYP/6-311+G*) level

Table 9. The reaction rate constants (cm^3/molecule/s) for the decomposition reaction LiN_5-B → TS2 → LiN_3+N_2

T (K)	TST	CVT	CVT/SCT
250.0	1.5729×10^{-2}	1.4047×10^{-2}	1.7099×10^{-1}
298.0	5.0754	4.2282	2.3679×10^{1}
350.0	4.6188×10^{2}	3.6062×10^{2}	1.2313×10^{3}
400.0	1.2012×10^{4}	8.9040×10^{3}	2.2434×10^{4}
450.0	1.5413×10^{5}	1.0942×10^{5}	2.2379×10^{5}
500.0	1.2014×10^{6}	8.2259×10^{5}	1.4489×10^{6}
600.0	2.6678×10^{7}	1.7266×10^{7}	2.5035×10^{7}
700.0	2.4793×10^{8}	1.5396×10^{8}	1.9868×10^{8}
800.0	1.3297×10^{9}	8.0023×10^{8}	9.5847×10^{8}
1,000.0	1.4102×10^{10}	1.3610×10^{10}	1.4978×10^{10}
1,250.0	9.3938×10^{10}	8.7236×10^{10}	9.1422×10^{10}
1,500.0	3.3358×10^{11}	3.0188×10^{11}	3.0867×10^{11}

Table 10. The reaction rate constants (cm^3/molecule$^-$/s) for the decomposition reaction NaN_5-B → TS4 → NaN_3+N_2

T (K)	TST	CVT	CVT/SCT
250.0	5.6030×10^{-5}	5.3578×10^{-5}	3.9320×10^{-3}
298.0	4.5213×10^{-2}	4.3563×10^{-2}	1.0328
350.0	8.3911	8.1337	9.2528×10^{1}
400.0	3.6427×10^{2}	3.5466×10^{2}	2.5125×10^{3}
450.0	6.9700×10^{3}	6.8100×10^{3}	3.4265×10^{4}
500.0	7.4834×10^{4}	7.3325×10^{4}	2.8511×10^{5}
600.0	2.6893×10^{6}	2.6463×10^{6}	7.1862×10^{6}
700.0	3.5267×10^{7}	3.4808×10^{7}	7.4810×10^{7}
800.0	2.4495×10^{8}	2.4229×10^{8}	4.4322×10^{8}
1,000.0	3.7313×10^{9}	3.7018×10^{9}	5.5354×10^{9}
1,250.0	3.3211×10^{10}	3.3021×10^{10}	4.3037×10^{10}
1,500.0	1.4307×10^{11}	1.4244×10^{11}	1.7173×10^{11}

Table 11. The reaction rate constants (cm^3/molecule$^-$/s$^-$) for the decomposition reaction KN_5-B → TS6 → KN_3+N_2

T (K)	TST	CVT	CVT/SCT
250.0	1.5128×10^{-5}	3.8066×10^{-6}	1.3014×10^{-2}
298.0	1.4822×10^{-2}	$3.6230E\times10^{-3}$	3.2355×10^{-2}
350.0	3.1979	7.6445×10^{-1}	1.0884
400.0	1.5468×10^{2}	3.6415×10^{1}	3.9523×10^{1}
450.0	3.2197×10^{3}	7.4962×10^{2}	7.0945×10^{2}
500.0	3.6984×10^{4}	8.5404×10^{3}	7.3959×10^{3}
600.0	1.4710×10^{6}	3.3611×10^{5}	2.6244×10^{5}
700.0	2.0745×10^{7}	4.7123×10^{6}	3.4956×10^{6}
800.0	1.5218×10^{8}	3.4459×10^{7}	2.4944×10^{7}
1,000.0	2.5030×10^{9}	5.6562×10^{8}	4.0502×10^{8}
1,250.0	2.3693×10^{10}	5.3599×10^{9}	3.8925×10^{9}
1,500.0	1.0635×10^{11}	2.4121×10^{10}	1.7912×10^{10}

Table 12. The reaction rate constants (cm^3/molecule/s) for the decomposition reaction RbN_5-B → TS8 → RbN_3+N_2

T (K)	TST	CVT	CVT/SCT
250.0	5.4546×10^{-6}	5.4210×10^{-6}	3.1626
298.0	6.3493×10^{-3}	6.3235×10^{-3}	5.6253
350.0	1.5658	1.5618	2.2702×10^{1}
400.0	8.3358×10^{1}	8.3236×10^{1}	3.9822×10^{2}
450.0	1.8698×10^{3}	1.8684×10^{3}	6.1754×10^{3}
500.0	2.2803×10^{4}	2.2795×10^{4}	6.0056×10^{4}
600.0	9.9224×10^{5}	9.9223×10^{5}	1.9599×10^{6}
700.0	1.4921×10^{7}	1.4919×10^{7}	2.4709×10^{7}
800.0	1.1486×10^{8}	1.1479×10^{8}	1.6915×10^{8}
1,000.0	2.0209×10^{9}	2.0172×10^{9}	2.5806×10^{9}
1,250.0	2.0189×10^{10}	2.0113×10^{10}	2.3425×10^{10}
1,500.0	9.3936×10^{10}	8.2784×10^{10}	5.4935×10^{10}

Acknowledgements. The authors thank D.G. Truhlar for providing the Polyrate 8.2 program. J.F.Z. thanks R.H. Lü and S.W. Zhang for their help with the use of the Polyrate program and the analyses of the computed results.

References

1. Pyykkö P, Runeberg J (1991) J Mol. Struct (THEOCHEM) 234:279
2. Yarkony DR (1992) J Am Chem Soc 114:5406
3. Glukhovtsev MN, Jiao H, Schleyer PvR (1996) Inorg Chem 35:7124

4. Bartlett RJ (2000) Chem Ind 4:140
5. Nguyen MT, Ha T-K (2001) Chem Phys Lett 335:311
6. Workentin MS, Wagner BD, Lusztyk J, Wayner DM (1995) J Am Chem Soc 117:119
7. Gagliardi L, Orlandi G, Evangelisti S, Roos BO (2001) J Chem Phys 114:10733
8. Michels HH, MontgomeryJA Jr, Christe KO, Dixon DA(1995) J Phys Chem 99:187
9. Hammerl A, Klapötke TM (2002) Inorg Chem 41:906
10. Olah GA, Prakash GKS, Rasul G (2001) J Am Chem Soc 123:3308
11. Christe KO, Wilson WW, Sheehy JA, Boatz JA (1999) Angew Chem Int Ed Engl 38:2004
12. Cacace F, Petris G, Troiani A(2002) Science 295:480
13. Vij A, Pavlovich J.G, Wilson WW, Vij V, Christe KO (2002) Angew Chem Int Ed Engl 41:3051
14. Ferris KF, Bartlett RJ (1992) J Am Chem Soc 114:8302
15. Glukhovtsev MN, Schleyer PvR, Maerker C (1993) J Phys Chem 97:8200
16. Nguyen MT, McGinn MA, Hegarty AF, Elguero J (1985) Polyhedron 4:1721
17. Gagliardi L, Pykkö P (2001) J Am Chem Soc 123:9700
18. Gagliardi L, Pykkö P (2002) J Phys Chem A 106:4690
19. Lein M, Frunzke J, Timoshkin A, Frenking G (2001) Chem Eur J 7:4155
20. Burke LA, Butler RN, Stephens JC (2001) J Chem Soc Perkin Trans 2:1679
21. Frisch MJ et al. (1998) GAUSSIAN 98, revision A.9. Gaussian, Pittsburgh, PA
22. Becke AD (1993) J Chem Phys 98:5648
23. Lee C, Yang W, Parr RG (1988) Phys Rev B 37:785
24. Perdew JP, Wang Y (1998) Phys Rev B 37:785
25. Andrae D, Haeussermann U, Dolg M, Stoll H, Preuss H (1990) Theor Chim Acta 77:123
26. Nicklass A, Dolg M, Stoll H, Preuss H (1995) J Chem Phys 102:8942
27. Leininger T, Nicklass A, Stoll H, Dolg M, Schwerdtfeger P (1996) J Chem Phys 105:1052
28. Gonzalez C, Schlegel HB (1989) J Chem Phys 90:2154
29. Gonzalez C, Schlegel HB (1990) J Phys Chem 94:5523
30. Carpenter JE, Weinhold F (1988) J Mol Struct (THEOCHEM) 169:41
31. Carpenter JE (1987) PhD thesis. University of Wisconsin, Madison
32. Stickler R, Hu W-P et al. (1995) Comput Phys Commum 88:341
33. Lide DR (ed) (1992–1993) CRC handbook of chemistry and physics, 73rd edn. CRC, Boca Raton, pp 9–31
34. King CM, Nixon ER (1968) J Phys Chem 48:1685
35. Feller D (1992) J Chem Phys 96:6104